Chapter

Guidance and Control of a Planar Robot Manipulator Used in an Assembly Line

Bülent Özkan

Abstract

In order to achieve higher productivity and lower cost requirements, robot manipulators have been enrolled in assembling processes in last decades as well as other implementation areas such as transportation, welding, mounting, and quality control. As a new application of this field, the control of the synchronous movements of a planar robot manipulator and moving belt is dealt with in this study. Here, the mentioned synchronization is tried to be maintained in accordance with a guidance law which leads the robot manipulator to put selected components onto the specific slots on the moving belt without interrupting the assembling process. In this scheme, the control of the manipulator is carried out by considering the PI (proportional plus integral) control law. Having performed the relevant computer simulations based on the engagement geometry between the robot manipulator and moving belt, it is verified that the mentioned pick-and-place task can be successfully accomplished under different operating conditions.

Keywords: Guidance and control, robot manipulator, linear homing guidance law, assembly line, automation

1. Introduction

Robot manipulators have been utilized in many application areas since 1960's [1, 2]. In addition to their implementations in harsh and unusual environments involving tedious, hard, and hazardous tasks, the productivity, cost reduction, and time effectiveness considerations have put forward the use of the manipulators in the production and assembly applications [3–5].

Regarding the pick-and-place operations in which certain components are placed onto specific slots on a moving belt by means of the end effector of the robot manipulator that constitute the hand of the manipulator, the most common method is to make the placement of the component to the slot once they coincide. This attitude has been chosen by some famous vehicle manufacturers [6]. Since it is required to halt the moving belt at coincidences of the end effector of the robot and slot in this scheme, a discrete motion strategy is developed for this purpose. Even though this approach works well when relatively light components are under consideration, the increment in the component mass leads to higher acceleration requirements to speed up the belt right after the placement. In such a scheme with a robot manipulator, the belt should be halted at specific points in order to allow the

manipulator to put the component on the slot. In fact, this means using powerful actuators which are big and expensive in practice and hence it violates the cheapness demand.

As a remedy to the preceding method, it seems reasonable to the motion of the belt even during placement. This results in diminishing the power need in operation and allows to use smaller and cheaper actuators, or motors [7]. On the other hand, it may not possible to coincide the end effector of the robot manipulator grasping the components and belt all the time due to uncertain factors such as nonlinear friction effects on the belt dynamics when larger and heavier parts are considered as in automotive industry. In order to compensate this weakness of conventional motion planning strategies based on making the placements upon the pre-calculated coincidence positions ignoring the probable uncertainties, "guidance" approach can be utilized in continuous-time engagements.

In addition to optimization-based motion planning schemes based on the minimum time and/or minimum energy expenditure criteria, a hybrid target point interception algorithm is proposed as schematized in **Figure 1** where the abbreviation AIPNG stands for the "augmented ideal proportional navigation guidance" for target catching [8–12]. In the mentioned studies in which the position information is often acquired by visual sensors, the engagement models including planar manipulators having two or three degrees of freedom, or two or three links, in general are validated through computer simulations [13, 14].

Guidance laws developed originally for the munitions against specific targets can be adapted to the motion planning of the robot manipulators that can be thought as "very short-range missiles" regarding their connections to the ground [15]. As an advantage over the munitions which have generally no thrust support during their guidance phase, the robot manipulators can be accelerated along their longitudinal axis [13]. In early applications, the robotic arms were tried to be guided by means of certain sensors placed on the end effectors such as optical sensors operating along with laser beams and visual sensors, i.e. cameras [16, 17]. As a distinguished implementation of guided robot manipulators, the guidance of micromanipulators utilized in microsurgery is accomplished by the visual guidance of the operator, i.e. surgeon [18]. The vision-based guidance approach is proposed for tele-robotic systems as well [2]. Moreover, the guidance of mobile robots is dealt with in swarm arrangements [19]. In another robotic application, the proportional navigation

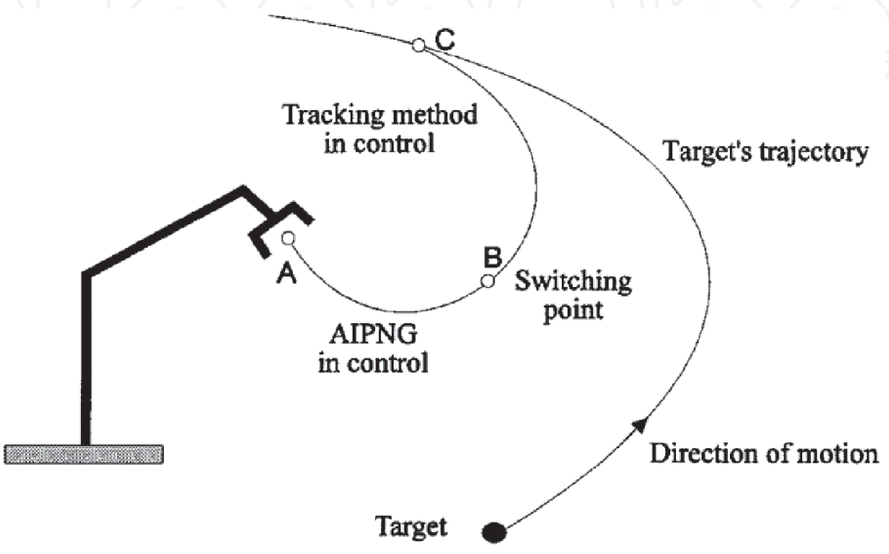

Figure 1.
Hybrid target interception scheme [8].

guidance (PNG) law which is very popular in aerial systems is considered with different navigation constants under the absence and presence of obstacles on the collision trajectory between the manipulator and target object and relative computer simulations are performed [20].

In order to synchronize the movements of the robot manipulator and moving belt in a continuous operation, it is a viable way to make them compatible in speed sense. This solution reduces to order of the robot manipulator dynamics two to one and thus most of the overshoots in the transient motion phase of the manipulator can be prevented [21].

The control strategy is very significant for the realization of commands generated by the considered guidance law. For this purpose, certain control methods are encountered in the literature for the robot manipulators such as H_2/H_∞ norm-based robust control scheme supplemented by a Takagi-Sugeno type fuzzy control such that parameter uncertainties and nonlinear effects are accounted [22]. Similar to this work, the control of a prosthetic leg is handled regarding a stable robust adaptive impedance control [23]. The adaptive control of robot manipulators has become one of the most popular research areas for last decades. The control schemes based on classical laws such as PD (proportional plus derivative) law are proposed against parameter uncertainties and unmodeled disturbances. The effectiveness of the suggested approaches is then tried to be demonstrated by well-designed computer simulations and experimental studies [24, 25].

In this study, a guidance-based motion planning approach utilizing the linear homing guidance (LHG) law is proposed for the engagement problem between a planar two-link robot manipulator shown in **Figure 2** with an origin point O and moving belt in a continuous manner [20]. Although the LHG law generates the guidance commands in terms of the linear velocity components of the tip point of the manipulator, it is more reasonable to control the manipulator through the corresponding joint variables because the actuators are connected to the joints. Therefore, an indirect adaptive control system based on the computer torque method is designed by continuously updating the controller gains during the operation after transforming the guidance commands to the joint space [13, 26]. As per the data acquired from the computer simulations conducted in the MATLAB®

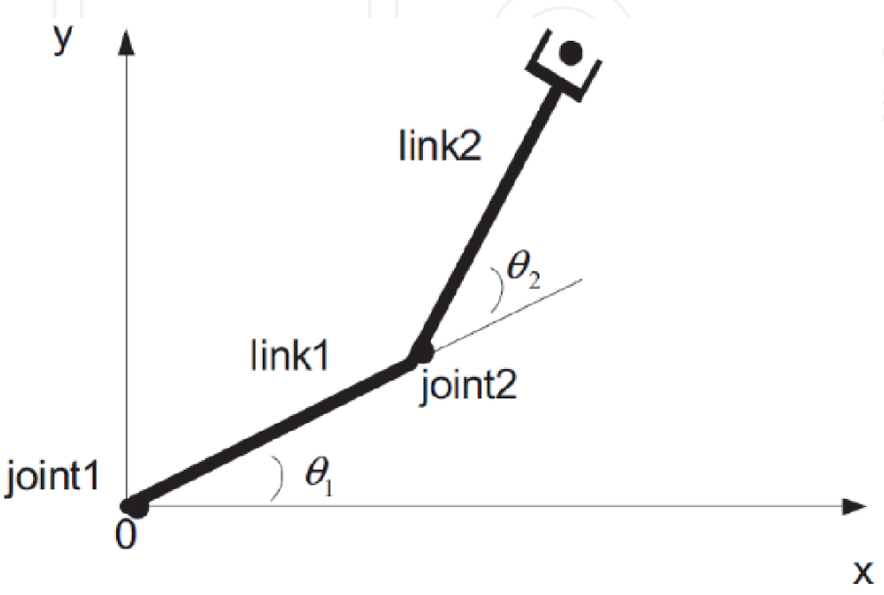

Figure 2.
Two-link robot manipulator [9].

SIMULINK® environment, it is decided that the present approach can be applied on mounting lines to attain affordable and cheaper processes.

2. System Definition

Taking the component as a two degrees of freedom spherical mass whose position is fully defined by the horizontal and lateral linear position components of a point on it, i.e. point *P*, at any time with no orientation, it suffices to have a robot manipulator with two degrees of freedom to move the component to any point on the horizontal plane within its kinematic limits. The schematic view of the system involving the two-link robot manipulator and moving belt is submitted in **Figure 3** along with the corresponding definitions listed below.

x and *y*: horizontal and lateral axes of the inertial frame represented by F_0.

$\vec{u}_1^{(0)}$ and $\vec{u}_2^{(0)}$: unit vectors denoting the *x* and *y* axes of F_0.

O and *A*: joints of the robot manipulator.

a_1 and a_2: lengths of the first and second links of the robot manipulator.

θ_1 and θ_2: relative rotation angles of the first and second joints of the robot manipulator.

P: point taken on the end effector of the robot manipulator.

x_P and y_P: horizontal and lateral position components of point *P*.

S: mid-point of the slot on the moving belt.

S_i: changing points of the shape of the moving belt (i = 1, 2, 3, and 4).

v_S: speed of the slot on the moving belt.

x_S and y_S: horizontal and lateral position components of point *S*.

ρ: turn radius of the moving belt.

ψ: rotation angles of the moving belt on its circular tip portions.

L: total length of the moving belt.

d: perpendicular distance between the connection point of the robot manipulator to the ground and the center line of the portion of the moving belt in the closest position to that point.

$\vec{g}$: gravity vector (g = 9.81 m/s^2).

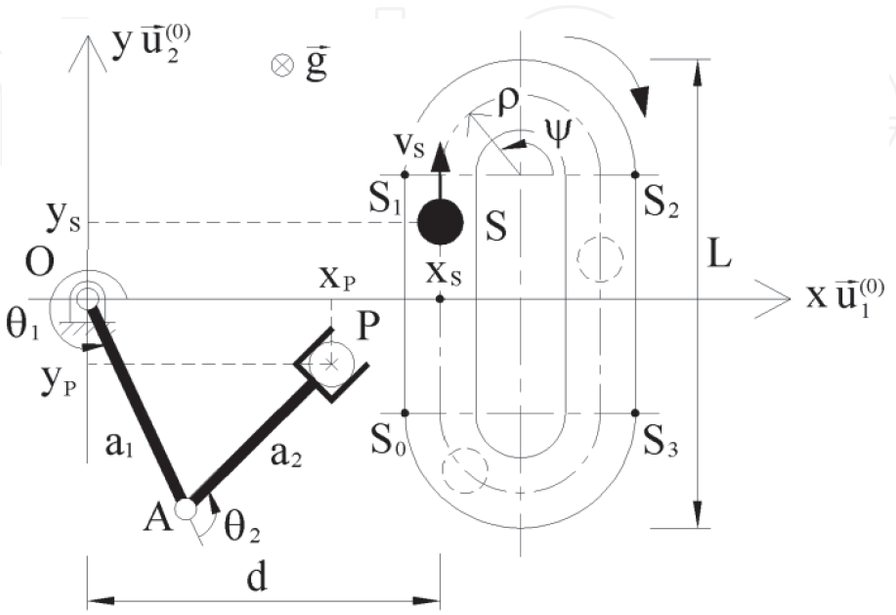

Figure 3.
System of the robot manipulator and moving belt.

3. Robot Manipulator Kinematics

In order to transform the guidance commands to the linear velocity components of the manipulator tip point into the angular speed variables of the joints, the kinematic relationships among those variables are considered.

Thus, the column vector of the position components of point P on the end effector ($\overline{r}_P$) can be written in terms of θ_1 andθ_2 in the next manner:

$$\overline{r}_P = a_1 e^{j\theta_1} + a_2 e^{j\theta_{12}} \tag{1}$$

where $\overline{r}_P = \begin{bmatrix} x_P & y_P \end{bmatrix}^T$ and $\theta_{12} = \theta_1 + \theta_2$ with $j = \sqrt{-1}$ while the letter "e" stands for the "exponential" operation.

Resolving Eq. (1) into its components, the equations given below come into the picture:

$$x_P = a_1 \cos(\theta_1) + a_2 \cos(\theta_{12}) \tag{2}$$

$$y_P = a_1 \sin(\theta_1) + a_2 \sin(\theta_{12}) \tag{3}$$

In velocity level, the following matrix expression is found by taking the time derivative of Eq. (1) with $\overline{\theta} = \begin{bmatrix} \theta_1 & \theta_2 \end{bmatrix}^T$:

$$\dot{\overline{r}}_P = \hat{J}_P \dot{\overline{\theta}} \tag{4}$$

In Eq. (4), the Jacobian matrix of the manipulator tip point is defined as follows:

$$\hat{J}_P = \begin{bmatrix} -a_1 \sin(\theta_1) - a_2 \sin(\theta_{12}) & -a_2 \sin(\theta_{12}) \\ a_1 \cos(\theta_1) + a_2 \cos(\theta_{12}) & a_2 \cos(\theta_{12}) \end{bmatrix} \tag{5}$$

From Eq. (4), the angular velocities of the manipulator links can be obtained as given below:

$$\dot{\overline{\theta}} = \hat{J}_P^{-1} \dot{\overline{r}}_P \tag{6}$$

The "elbow-up" configuration of the manipulator in which the joint indicated by letter A in **Figure 3** becomes in the upper position is taken into account in the inverse kinematic calculation above.

Eventually, the linear acceleration equations come into the picture by taking the time derivative of Eq. (6):

$$\ddot{\overline{\theta}} = \hat{J}_P^{-1} \left(\ddot{\overline{r}}_P - \dot{\hat{J}}_P \dot{\overline{\theta}} \right) \tag{7}$$

In Eq. (7), the time derivative of the tip point Jacobian matrix are determined in the forthcoming fashion with $\dot{\theta}_{12} = \dot{\theta}_1 + \dot{\theta}_2$:

$$\dot{\hat{J}}_P = \begin{bmatrix} -a_1 \dot{\theta}_1 \cos(\theta_1) - a_2 \dot{\theta}_{12} \cos(\theta_{12}) & -a_2 \dot{\theta}_{12} \cos(\theta_{12}) \\ -a_1 \dot{\theta}_1 \sin(\theta_1) - a_2 \dot{\theta}_{12} \sin(\theta_{12}) & -a_2 \dot{\theta}_{12} \sin(\theta_{12}) \end{bmatrix} \tag{8}$$

4. Dynamic Modeling of the Robot Manipulator

The governing differential equations of motion of the robot manipulator schematized in **Figure 3** can be derived using the well-known virtual work method [9].

Neglecting the gravity vector ($\vec{g}$) for the present engagement described on the horizontal plane, the equations of motion of the manipulator can be derived in the matrix form as follows:

$$\overline{T} = \hat{M}(\overline{\theta})\,\ddot{\overline{\theta}} + \hat{H}\left(\dot{\overline{\theta}}, \overline{\theta}\right)\dot{\overline{\theta}} \tag{9}$$

In Eq. (9), $\overline{T} = [\,T_1 \quad T_2\,]^T$ stands for the torque column matrix with T_1 and T_2 which denote the control torques applied to the first and second joints of the robot manipulator, respectively. Here, the superscript "T" indicates the "transpose" operation. Also, the inertia and compound friction and Coriolis matrices [$\hat{M}(\overline{\theta})$ and $\hat{H}\left(\dot{\overline{\theta}}, \overline{\theta}\right)$] are introduced in the following manner:

$$\hat{M}(\overline{\theta}) = \begin{bmatrix} m_{11} & m_{12} \\ m_{12} & m_{22} \end{bmatrix} \tag{10}$$

$$\hat{H}\left(\dot{\overline{\theta}}, \overline{\theta}\right) = \begin{bmatrix} h_{11} & h_{12} \\ h_{21} & h_{22} \end{bmatrix} \tag{11}$$

where m_1, m_2, I_{c1}, and I_{c2} correspond to the masses of the first and second links of the manipulator, and the moments of inertia of these links with respect to their mass centers indicated by C_1 and C_2, respectively. Moreover, b_1 and b_2 are used to show the viscous friction coefficients at the first and second joints. With the definitions of $d_1 = |O\,C_1|$ and $d_2 = |A\,C_2|$ as additional length parameters, the following symbols are used in Eqs. (10) and (11).

$$\begin{aligned} m_{11} &= m_1 d_1^2 + m_2\left[a_1^2 + d_2^2 + 2a_1 d_2\cos(\theta_2)\right] + I_{c1} + I_{c2}, m_{12} \\ &= m_2 d_2\left[d_2 + a_1\cos(\theta_2)\right] + I_{c2}, m_{22} = m_2 d_2^2 + I_{c2}, h_{11} \\ &= b_1 - 2m_2 a_1 d_2\dot{\theta}_2\sin(\theta_2), h_{12} = b_2 - m_2 a_1 d_2\dot{\theta}_2\sin(\theta_2), h_{21} \\ &= m_2 a_1 d_2\dot{\theta}_1\sin(\theta_2), \text{and } h_{22} = b_2. \end{aligned}$$

Substituting Eqs. (10) and (11) into Eq. (9), the following expressions are determined for T_1 and T_2, respectively:

$$\begin{aligned} T_1 = {} & \left[m_1 d_1^2 + m_2\left(a_1^2 + d_2^2 + 2a_1 d_2\cos(\theta_2)\right) + I_{c1} + I_{c2}\right]\ddot{\theta}_1 \\ & + \left[m_2 d_2\left(d_2 + a_1\cos(\theta_2)\right) + I_{c2}\right]\ddot{\theta}_2 + b_1\dot{\theta}_1 + b_2\dot{\theta}_2 \\ & - m_2 a_1 d_2\left(2\dot{\theta}_1\dot{\theta}_2 + \dot{\theta}_2^2\right)\sin(\theta_2) \end{aligned} \tag{12}$$

$$\begin{aligned} T_2 = {} & \left[m_2 d_2\left(d_2 + a_1\cos(\theta_2)\right) + I_{c2}\right]\ddot{\theta}_1 + \left(m_2 d_2^2 + I_{c2}\right)\ddot{\theta}_2 \\ & + b_2\dot{\theta}_2 + m_2 a_1 d_2\dot{\theta}_1^2\sin(\theta_2) \end{aligned} \tag{13}$$

5. Robot manipulator control system

In order to keep the synchronization between the robot manipulator and moving belt during their engagement, it is more viable to make the control of the manipulator by considering its speed. That is, the components of the linear velocity vector of point P on the end effector of the manipulator in the horizontal plane become the parameters which should actually be controlled in a manner compatible with the command signals of the LHG law that are in the form of speed variables. On the

other hand, it is easier and more practical to measure the joint speeds ($\dot{\theta}_1$ and $\dot{\theta}_2$) than the linear velocity components of point P. For this reason, an indirect control scheme is designed in the present study such that the joint speeds are selected as control variables. In this situation, it is required to express the linear velocity components of point *P* in terms of the joint speeds. Here, the linear position and velocity components of point *P* can be calculated from Eqs. (2) through (4) using the measured joint angles and their rates.

Introducing $\dot{\theta}_{1d}$ and $\dot{\theta}_{2d}$ to demonstrate the desired, or reference, joint speeds with the column matrix $\dot{\overline{\theta}}_d = \begin{bmatrix} \dot{\theta}_{1d} & \dot{\theta}_{2d} \end{bmatrix}^T$, the error column matrix between the desired and actual joint speeds ($\overline{e}$) can be introduced as follows:

$$\overline{e} = \dot{\overline{\theta}}_d - \dot{\overline{\theta}} \tag{14}$$

In order to make the steady state errors zero, the following control law including an integral action is designating upon the torque input of the manipulator as per the computed torque method [27–29]:

$$\overline{T} = \hat{M}\ddot{\overline{\theta}}_d + \hat{H}\dot{\overline{\theta}} + \hat{K}_p\overline{e} + \hat{K}_i\int \overline{e}\,dt \tag{15}$$

where $\hat{M} = \hat{M}(\overline{\theta})$ and $\hat{H} = \hat{H}\left(\dot{\overline{\theta}}, \overline{\theta}\right)$ are defined. Also, $\hat{K}_p$ and $\hat{K}_i$ stand for the proportional and integral gain matrices, respectively, and $\hat{M}$ and $\hat{H}$ matrices are assumed to be accurately calculated. As can be seen, the proposed control system is based on the PI (proportional plus integral) control law [14, 30].

Inserting Eq. (15) into Eq. (9) and making the arrangements regarding Eq. (14), the error dynamics of the control system is obtained in the following manner:

$$\ddot{\overline{e}} + \hat{M}^{-1}\left(\dot{\hat{M}} + \hat{K}_p\right)\dot{\overline{e}} + \hat{M}^{-1}\hat{K}_i\overline{e} = \overline{0} \tag{16}$$

where $\dot{\hat{M}} = -m_2 a_1 d_2 \dot{\theta}_2 \sin(\theta_2)\begin{bmatrix} 2 & 1 \\ 1 & 0 \end{bmatrix}$.

For a finite solution, the existence of $\hat{M}^{-1}$ must be guaranteed by the invertible matrix $\hat{M}$. That is, the determinant of $\hat{M}$ must be nonzero. Here, the determinant of $\hat{M}$, i.e. $|\hat{M}|$, is obtained from Eq. (10) as follows:

$$|\hat{M}| = I_{c1}\left(m_1 d_1^2 + m_2 d_2^2 + I_{c2}\right) + m_2 a_1^2\left[m_2 d_2^2 \sin^2(\theta_2) + I_{c2}\right] + m_1 m_2 d_1^2 d_2^2 \tag{17}$$

As noticed, $|\hat{M}|$ never becomes zero unless any of the mass and inertia parameters of the links of the manipulators disappears. Because this is not possible in physical sense, $\hat{M}$ is invertible in all conditions and hence $\hat{M}^{-1}$ exists.

For a second-order two-degree-of-freedom ideal system, the error dynamics can be defined using the forthcoming expression as ω_{ci} and ζ_{ci} correspond to the bandwidth and damping parameters of the i^{th} link (i = 1 and 2), respectively [27]:

$$\ddot{\overline{e}} + \hat{D}\dot{\overline{e}} + \hat{W}\overline{e} = \overline{0} \tag{18}$$

where $\hat{D} = \begin{bmatrix} 2\zeta_{c1}\omega_{c1} & 0 \\ 0 & 2\zeta_{c2}\omega_{c2} \end{bmatrix}$ and $\hat{W} = \begin{bmatrix} \omega_{c1}^2 & 0 \\ 0 & \omega_{c2}^2 \end{bmatrix}$.

Finally, equating Eqs. (16) and (18) to each other, $\hat{K}_p$ and $\hat{K}_i$ appear as follows:

$$\hat{K}_p = \hat{M}\hat{D} - \dot{\hat{M}} \tag{19}$$

$$\hat{K}_i = \hat{M}\hat{W} \tag{20}$$

In order to maintain the stability of the manipulator control systems throughout the engagement, the components of the matrices $\hat{K}_p$ and $\hat{K}_i$ which may be diagonal or off-diagonal are updated at certain instants.

6. Moving belt kinematics

The horizontal and lateral position components of point S (x_S and y_S) showing the slot on the moving as shown in **Figure 3** are described at the changing points symbolized by S_i (i = 1, 2, 3, and 4) by taking v_S to be constant in the next manner:

$$(x_S, y_S) = \begin{cases} x_0, y_0 + v_s(t - t_0) & , \quad x_0 \le x_S < x_1 \\ x_1 + \rho[\cos(\psi) + 1], y_1 + \rho \sin(\psi) & , \quad x_1 \le x_S < x_2 \\ x_2, y_2 - v_s(t - t_2) & , \quad x_2 \le x_S < x_3 \\ x_3 + \rho[\cos(\psi) - 1], y_3 + \rho \sin(\psi) & , \quad x_3 \le x_S < x_0 \end{cases} \tag{21}$$

In Eq. (21), the position variables of point S at the S_i location quantities are found by considering the following terms with the corresponding rotation angle at these points (ψ_i) (π = 3.14):

$$x_0 = d, y_0 = \rho - (L/2), \psi_0 = \pi \text{ rad}; x_1 = d, y_1 = (L/2) - \rho, \psi_1 = \pi \text{ rad}; x_2 = d + 2\rho, y_2 = (L/2) - \rho, \psi_2 = 0; x_3 = d + 2\rho, y_3 = \rho - (L/2), \text{and } \psi_3 = 0.$$

where x_i, y_i, and t_i denote the horizontal and lateral position variables of point S at the S_i location, and time parameter, respectively.

In Eq. (21),ψ can be determined from the following expression as a function of time (t) for $t_1 = t_0 + (|y_1 - y_0|/v_S)$, $t_2 = t_1 + (\pi\rho/v_S)$, and $t_3 = t_2 + (|y_2 - y_3|/v_S)$ with a specified t0 value:

$$\psi = \begin{cases} \pi & , \quad x_0 \le x_s < x_1 \\ \pi - [v_S(t - t_1)/\rho] & , \quad x_1 \le x_s < x_2 \\ 0 & , \quad x_2 \le x_s < x_3 \\ 2\pi - [v_S(t - t_3)/\rho] & , \quad x_3 \le x_s < x_0 \end{cases} \text{(rad)} \tag{22}$$

7. Engagement geometry

The engagement geometry between point P on the end effector of the robot manipulator and point S carried by the moving belt can be schematized on the horizontal plane as given in **Figure 4**.

Introducing v_P, γ_m, $r_{S/P}$, γ_b, and λ as the magnitude of the resulting velocity vector of point P, orientation angle of v_P from the horizontal axis, relative position of point S with respect to point P, orientation angle of v_S from the horizontal axis, and angle between $r_{S/P}$ and horizontal axis in **Figure 4**, respectively, v_P, γ_b, and λ can be calculated using the equations below:

$$v_P = \sqrt{\dot{x}_P^2 + \dot{y}_P^2} \tag{23}$$

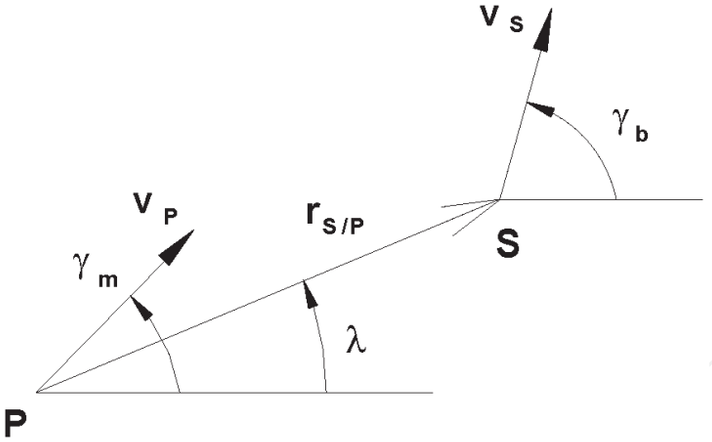

Figure 4.
Engagement geometry between the tip point of the manipulator and slot on the belt.

$$\gamma_b = \begin{cases} \pi/2 & , \quad x_0 \le x_S < x_1 \\ \psi - (\pi/2) & , \quad x_1 \le x_S < x_2 \\ -\pi/2 & , \quad x_2 \le x_S < x_3 \\ \psi - (\pi/2) & , \quad x_3 \le x_S < x_0 \end{cases} \text{(rad)} \tag{24}$$

$$\lambda = a\tan\left[\left(y_S - y_P\right)/\left(x_S - x_P\right)\right] \tag{25}$$

8. Guidance law

In the LHG law, it is intended to keep the end effector of the manipulator always on the collision triangle that is formed by the end effector, slot, and predicted intercept point. For this purpose, the most convenient approach is to orient the velocity vector of point P on the end effector ($\vec{v}_{Pactual}$) towards the predicted intercept point (I) at which the collision between the end effector and slot is going to be happen after a while as depicted in **Figure 5** with $\vec{v}_S$ and $\vec{v}_{Pideal}$ which denote the velocity of point S and the ideal velocity of point P [26].

In this law, in order for point P to catch point S, the guidance command (γ_m^c) is derived as follows [4, 26]:

$$\gamma_m^c = \lambda + a\sin\left[\left(v_S/v_P\right)\sin\left(\gamma_b - \lambda\right)\right] \tag{26}$$

Here, using the measurements of v_S by means of the appropriate sensors on the belt rollers, the position variables x_S, y_S, and ψ are obtained.

In the application, the following column matrix including the reference values of the linear velocity components of point P ($\dot{\bar{r}}_{Pd}$) are formed using γ_m^c:

$$\dot{\bar{r}}_{Pd} = v_P\left[\begin{array}{cc}\cos\left(\gamma_m^c\right) & \sin\left(\gamma_m^c\right)\end{array}\right]^T \tag{27}$$

In order to overcome the algebraic loop which occurs because the values of v_P and $\dot{\bar{r}}_d$ are dependent on each other, a nonzero value which is compatible with the current component-picking motion of the manipulator is assigned to v_P at the initiation of the engagement.

The guidance commands can be expressed in terms of the angular speeds by means of the next expression regarding Eqs. (6) and (27):

$$\dot{\bar{\theta}}_d = \hat{J}_P^{-1}\dot{\bar{r}}_{Pd} \tag{28}$$

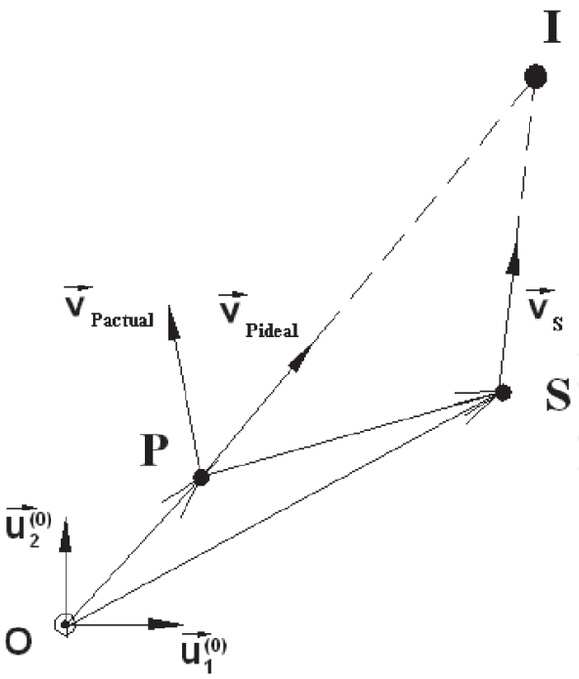

Figure 5.
Linear homing guidance law geometry.

9. Computer simulations

The numerical values considered in the computer simulations are submitted in **Table 1** along with the engagement block diagram in **Figure 6**.

The unit step responses at the first and second joints of the manipulator are submitted in **Figures 7** and **8** in which the discrete and continuous lines show the desired, or reference, and actual values of the joint angles, respectively. As shown, the desired joint speeds can be caught within the assigned bandwidth.

Parameter	Value	Parameter	Value	Parameter	Value
a_1 and a_2	1.25 m	b_1 and b_2	0.001 N·m·s/rad	L	2 m
d_1 and d_2	0.625 m	ω_{c1} and ω_{c2}	62.832 rad/s (=10 Hz)	ρ	0.5 m
m_1 and m_2	10 kg	ζ_{c1} and ζ_{c2}	0.707	d	1.5 m
I_{c1} and I_{c2}	1.302 kg·m^2				

Table 1.
Numerical values used in the computer simulations.

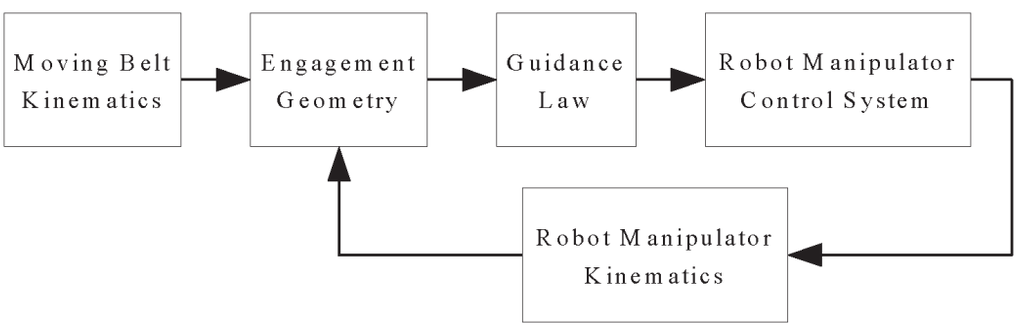

Figure 6.
Block diagram for the robot manipulator-moving belt.

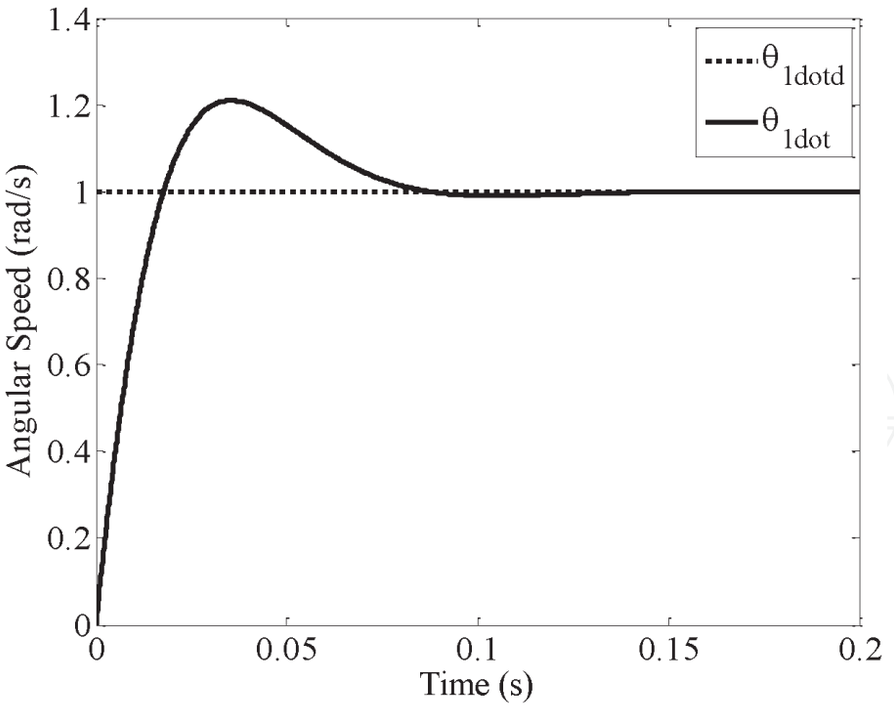

Figure 7.
Unit step response of the control system at the first joint.

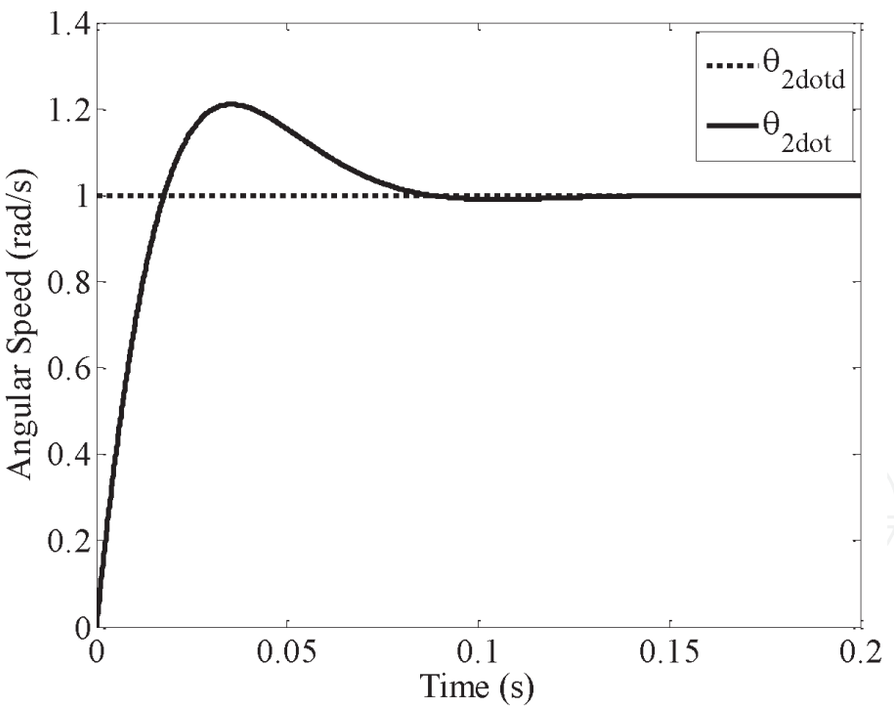

Figure 8.
Unit step response of the control system at the second joint.

In the designated engagement scenarios, it is assumed that the slot on the moving belt stands at point S_0 with $x_{S0} = 1.5$ and $y_{S0} = -0.5$ m at the instant when the robot manipulator is at rest. Furthermore, ramp-type angular speed inputs are applied to the manipulator joints in order for point P to attain its initial engagement velocity (v_{Pe}) at the end of 0.1 s. Here, the maximum angular speeds of the direct current (DC) electric motors connected to the joints are taken as 20 rad/s. The disturbance due to the nonlinear friction and noise on the sensors on the joints are

Conf. No.	Robot manipulator			Moving belt velocity (v_S) (m/s)
	Initial position of the tip point (m)		Velocity at the beginning of the engagement (v_{Pe}) (m/s)	
	x_{P0}	y_{P0}		
1	−0.5	−0.5	5.0×10^{-3}	0.5
2	−0.5	−0.5	5.0×10^{-3}	1.0
3	−0.5	−0.5	0.5	1.0
4	−1.0	−0.5	0.5	1.0
5	−1.0	−0.5	5×10^{-5}	2.5

Table 2.
Simulation configurations considered.

randomly varied in the ranges of ±10 N·m and $\pm 1 \times 10^{-3}$ rad, respectively. The solver is selected to be the ODE5 (Dormand-Prince)-type solver with a fixed time step of 1×10^{-4} s. The simulation configurations are designated as in **Table 2** along with the numerical values of the related parameters.

Having performed the computer simulations performed in the MATLAB® SIMULINK® environment, the results given in **Table 3** are attained. As samples, the engagement geometry for the configuration number 1 is given in **Figure 9** along with the plots for the changes of the velocity of point *P*, joint angles, joint speeds, and joint accelerations are submitted in **Figures 10–13**, respectively. Moreover, the engagement geometries for the sample configurations are plotted in **Figures 14** and **15**.

10. Discussion

As given in **Figures 9, 14**, and **15** which belong to the designated simulation configurations at belt speeds from 0.5 to 2.5 m/s, it is observed that the tip point of the manipulator can catch the slot on the moving belt even at higher speeds. In the present work, the slot is caught by the manipulator near the left side of the belt. Actually, this placement strategy is desired in order to diminish the power consumption of the robot manipulator by keeping the motion distance short compared to the distance to the right side of the belt. Looking at the simulation data which are presented in the forms of relevant kinematic parameters of the manipulator in **Figures 10–13**, it can be verified that the angular speed values required at the joints of the manipulator can be attained even with industrial DC electric motors as well as the angular excursion demands.

11. Conclusion

Motion planning constitutes one of the significant issues in the development of autonomous system. In this context, guidance concept has been applied on munition developed to satisfy precise hitting requirements for recent years. Both theoretical studies and field implementations have revealed that the guidance algorithms have led the relevant munition to the desired target points successfully. Of course, the performance of the designated guidance scheme is directly related to the control systems whose primary function is to obey the commands generated by the guidance law. For this purpose, several guidance and control approaches are

Conf. No.	Engagement time (s)	Maximum tip Point velocity (v_{Pmax}) (m/s)	Joint angles (°)				Joint speeds (rad/s)			
			θ_1		θ_2		$\dot{\theta}_1$		$\dot{\theta}_2$	
			Min.	Max.	Min.	Max.	Min.	Max.	Min.	Max.
1	0.299	31.339	−61.769	44.093	−159.876	−104.421	−6.127	20.161	−6.651	20.085
2	0.308	30.082	−62.451	52.147	−162.918	−106.102	−6.573	20.288	−8.469	20.202
3	0.267	30.654	−61.429	50.059	−161.766	−105.679	−6.268	21.158	−8.972	20.602
4	0.327	29.050	−90.000	54.134	−164.874	−106.239	−6.979	20.189	−17.313	20.106
5	0.745	25.000	−90.000	180.000	−164.369	−46.956	−20.146	0.000	−9.915	20.091

Table 3.
Results attained from the considered simulation configurations.

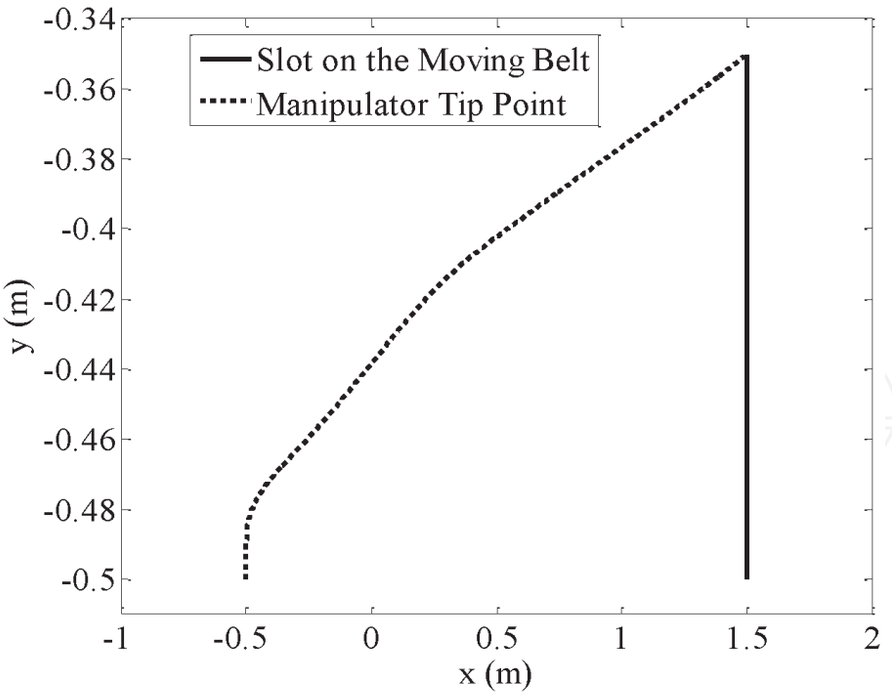

Figure 9.
Engagement geometry for the initial position components of the tip point of $x_{Po} = -0.5$ *m and* $y_{Po} = -0.5$ *m with a moving belt velocity of 0.5 m/s.*

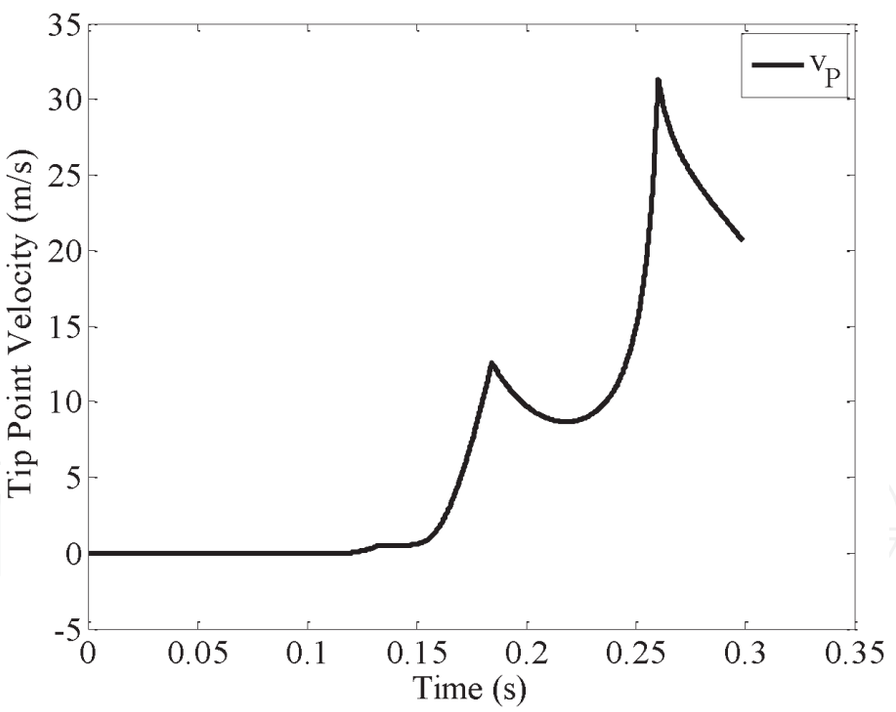

Figure 10.
Change of the velocity of point P in time for the initial position components of the tip point of $x_{Po} = -0.5$ *m and* $y_{Po} = -0.5$ *m with a moving belt velocity of 0.5 m/s.*

proposed depending on the kind of the planned mission as can be encountered in the related literature.

Regarding the fact that robot manipulators are designed to achieve certain tasks which are usually specified before the execution, it can be a viable way to apply the similar approach in munition for the motion planning tasks of the manipulators. As a result of the present work, it can be deduced that the guidance-based approach leads to a successful placement for the components onto the intended slots in

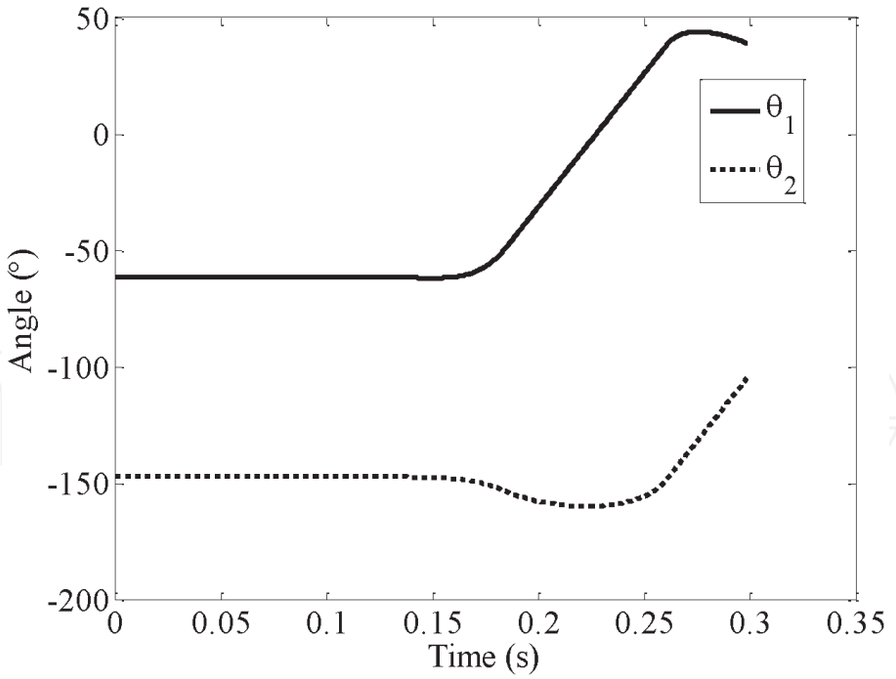

Figure 11.
Change of the joint angles in time for the initial position components of the tip point of $x_{Po} = -0.5$ *m and* $y_{Po} = -0.5$ *m with a moving belt velocity of 0.5 m/s.*

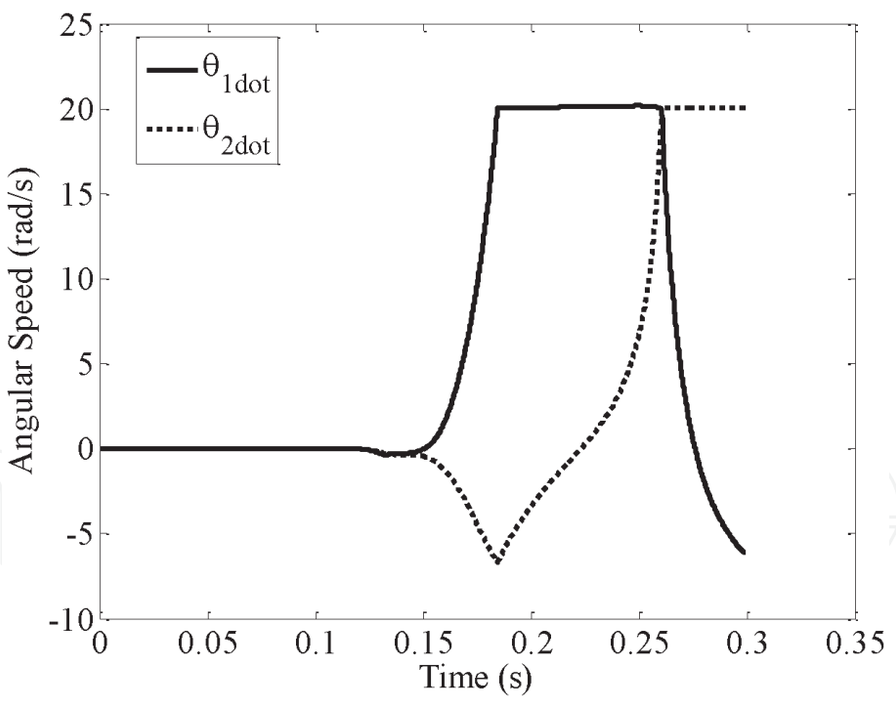

Figure 12.
Change of the joint speeds in time for the initial position components of the tip point of $x_{Po} = -0.5$ *m and* $y_{Po} = -0.5$ *m with a moving belt velocity of 0.5 m/s.*

continuous engagement operations. This can be done even under considerable disturbing effects and undesirable changing speed conditions of the belt with lower power consumption levels.

Although the applicability of the guidance and control approach on the robot manipulators is demonstrated by means of relevant computer simulations, there is not seen any serious difficulty to adapt the suggested concept into practice. This way, some of the robotic operations can be performed in an efficient manner.

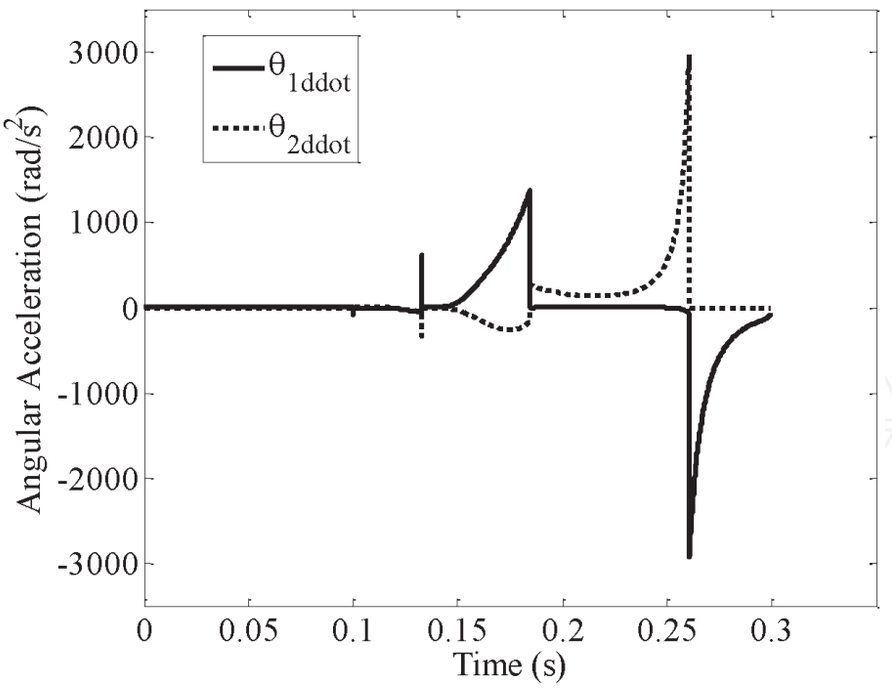

Figure 13.
Change of the joint accelerations in time for the initial position components of the tip point of $x_{Po} = -0.5$ *m and* $y_{Po} = -0.5$ *m with a moving belt velocity of 0.5 m/s.*

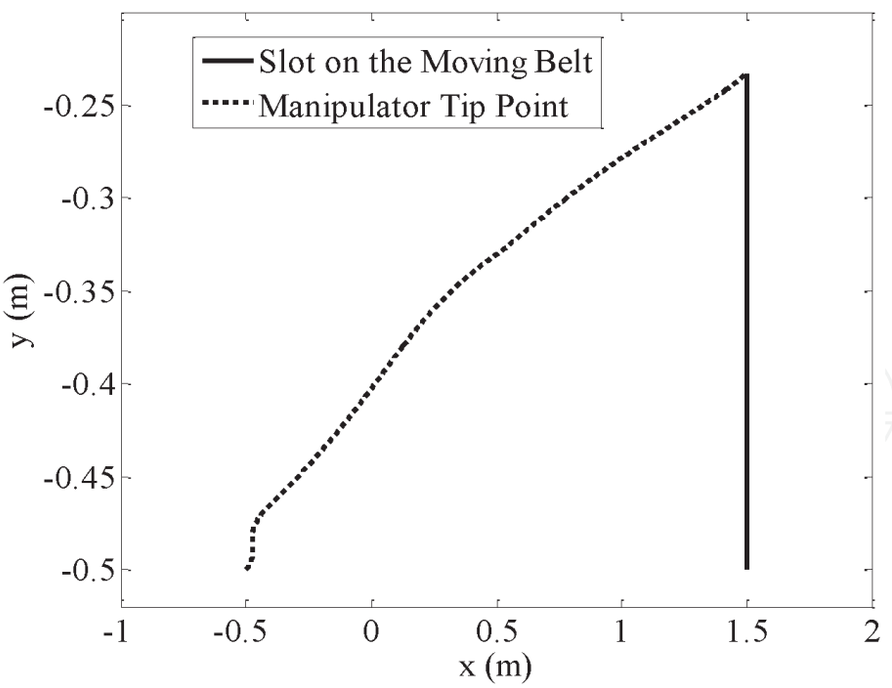

Figure 14.
Engagement geometry for the initial position components of the tip point of $x_{Po} = -0.5$ *m and* $y_{Po} = -0.5$ *m with a moving belt velocity of 1.0 m/s.*

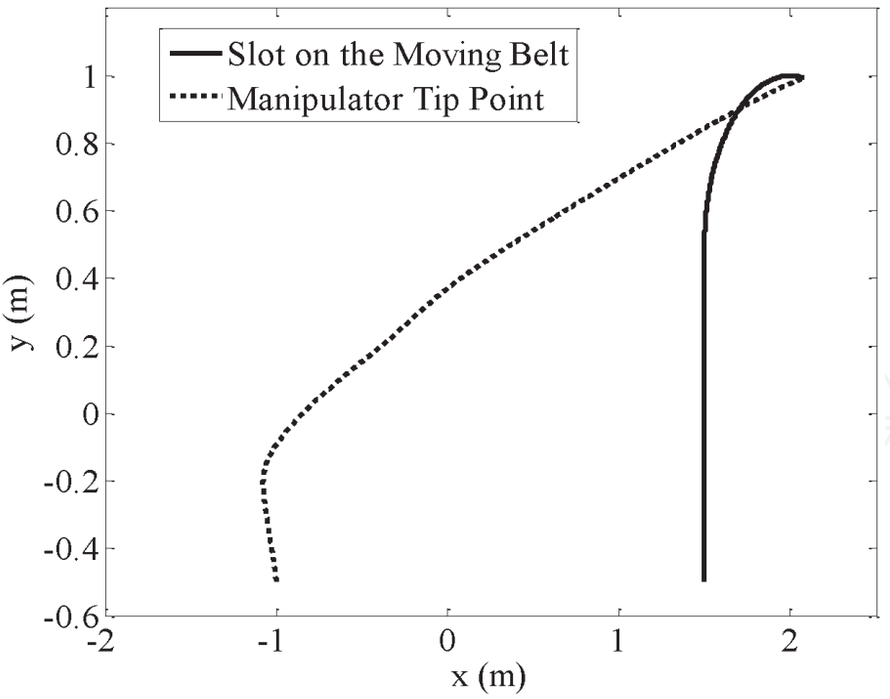

Figure 15.
Engagement geometry for the initial position components of the tip point of $x_{Po} = -1.0$ *m and* $y_{Po} = -0.5$ *m with a moving belt velocity of 2.5 m/s.*

Author details

Bülent Özkan
Mechanical Engineering Department, Gazi University, Ankara, Turkey

*Address all correspondence to: bozkan37@gmail.com

References

[1] Lan TS, Yeh LJ, Chiu MC, Hwang YX. Mint: Construction of the control system of cleaning robots with vision guidance. Mathematical Problems in Engineering. 2013;**2013**:1-6

[2] Ni T, Zhang H, Xu P, Yamada H. Mint: Vision-based virtual force guidance for tele-robotic system. Computers and Electrical Engineering. 2013;**39**:2135-2144

[3] Lewis FL. Abdallah. Dawson, DM. Control of Robot Manipulators: CT; 1993

[4] Özkan B. Guidance and control of a planar robot manipulator used in a mounting line. In: Proceedings of the 18th IFAC World Congress; 2011; Milan. Italy.

[5] Spong MW. Motion Control of Robot Manipulators-Control Handbook The Coordinated Science Laboratory. USA: University of Illinois at Urbana-Champaign; 2003

[6] İslamoğlu NE, Ryu K, Moon I. Mint: Labour productivity in modular assembly: a study of automotive module suppliers. International Journal of Production Research. 2014;**52**(23): 6954-6970

[7] Jang JS, Rim SC, Park SC. Mint: Reforming a conventional vehicle assembly plant for job enrichment. International Journal of Production Research. 2006;**44**(4):703-713

[8] Mehrandezh, M, Sela, MN, Fenton, RG, Benhabib, B. Proportional navigation guidance in robot trajectory planning for intercepting moving objects. In: Proceedings of the 1999 IEEE International Conference on Robotics and Automation; Detroit, Michigan, USA; 1999. p. 145–150

[9] Zhang Z, Wang WQ, Siddiqui S. Predictive function control of a two-arm robot manipulator. In: Proceedings of the IEEE International Conference on Mechatronics and Automation 2004-2009; 2005; Niagara Falls. Canada.

[10] Ferrara, A, Scattolini, R. Control of a robot manipulator for aerospace applications. In: Proceedings of the 6th Dynamics and Control of Systems and Structures in Space (DCSSS); Riomaggiore, Italy; 2004.

[11] Kunwar F, Benhabib B. Mint: Advanced predictive guidance navigation for mobile robots: a novel strategy for rendezvous in dynamic settings. International Journal on Smart Sensing and Intelligent Systems. 2008; **1**(4):858-890

[12] Mehrandezh, M. Navigation-guidance-based robot trajectory planning for ınterception of moving objects [thesis]. PhD Thesis, University of Toronto, Canada; 1999.

[13] Mehrandezh, M, Sela, NM, Fenton, RG, Benhabib, B. Mint: Robotic interception of moving objects using an augmented ideal proportional navigation guidance technique. IEEE Transcations on Systems, Man, and Cybernetics-Part A: Systems and Humans. 2000:30:3:238–250.

[14] Caner U, Eroğlu M. Mint: State feedback plus ıntegral error controller approach for robot arm control design (in Turkish). Journal of the Faculty of Engineering and Architecture of Gazi University. 2004;**19**(3):335-342

[15] Zarchan, P. Tactical and Strategic Missile Guidance. Vol. 157. Progress in Aeronautics and Astronautics, AIAA. Washington DC; USA; 1994.

[16] Koren Y, Shoham M. Mint: End-effector guidance of robot arms. Annals of the CIRP. 1987;**36**(1):289-292

[17] Garcia, GJ, Gil, P, Llácer, D, Torres, F. Guidance of robot arms using depth data from RGB-D camera. In: ICINCO 2013-10th International Conference on Informatics in Control, Automation and Robotics; 2013; Reykjavík, Iceland; p. 315–321.

[18] Becker BC, Voros S, MacLachlan RA, Hager GD, Riviere CN. Active guidance of a handheld micromanipulator using visual servoing. In: Proceedings of the IEEE International Conference on Robotics and Automation-2009 (ICRA'09); 2009; Kobe. Japan.

[19] Park JG, Shin JH. Mint: Autonomous navigation for a mobile robot using navigation guidance direction and fuzzy control. The Transactions of the Korean Institute of Electrical Engineers. 2014; **63**(1):108-114

[20] Belkhouche F, Rastgoufard P, Belkhouche B. Mint: Robot navigation-tracking of moving objects using the standard proportional navigation law. IEEE Trans. Robotics. 2007;**01**

[21] Seeraji S, Ovy EG, Alam T, Zamee A, Emon ARA. Mint: A flexible closed loop PMDC motor speed control system for precise positioning. International Journal of Robotics and Automation. 2011;**2**(3):211-219

[22] Azimi V, Menhaj MB, Fakharian A. Mint: Tool position tracking control of a nonlinear uncertain flexible robot manipulator by using robust H2/H∞ controller via T-S fuzzy model. Sadhana. 2015;**40**(2):307-333

[23] Azimi, V, Simon, D, Richter, H. Stable robust adaptive impedance control of a prosthetic leg. In: Proceedings of the ASME Dynamic Systems and Control Conference. Columbus. USA: Ohio; 2015

[24] Slotine JJE, Coetsee JA. Mint: Composite adaptive controller of robot manipulators. Automatica. 1989;**25**(4): 509-519

[25] Slotine JJE, Li W. Mint: Adaptive manipulator control: a study case. IEEE Transactions on Automatic Control. 1988;**33**(11):995-1003

[26] Özkan B, Özgören MK, Mahmutyazıcıoğlu G. Implementation of linear homing guidance law on a two-part homing missile. In: Proceedings of the 17th IFAC World Congress; 2008; Seoul. Republic of Korea.

[27] Ogata, K. Modern Control Engineering. 2nd ed.; Prentice-Hall International Editions; 1990.

[28] Bevly D, Dubovsky S, Mavroidis C. Mint: A simplified cartesian-computed torque controller for highly geared systems and its application to an experimental climbing robot. Journal of Dynamic Systems, Measurement, Control. 2000;**122**

[29] Yang Z, Wu J, Mei J, Gao J, Huang T. Mint: Mechatronic model based computed torque control of a parallel manipulator. International Journal of Advanced Robotic Systems. 2008;**5**(1):123-128

[30] Koca H, Doğan M, Taplamacıoğlu MC. Mint: Cartesian-specific control of a robot manipulator (in Turkish). Journal of the Faculty of Engineering and Architecture of Gazi University. 2008;**23**(4):769-776